Published in IET Electric Power Applications
Received on 13th November 2009
Revised on 2nd March 2010
doi: 10.1049/iet-epa.2009.0267

ISSN 1751-8660

Analysis of magnetic field distribution of a cylindrical discrete Halbach permanent magnet linear generator

Wijono H. Arof H.W. Ping

Department of Electrical Engineering, Faculty of Engineering, University of Malaya, 50603 Kuala Lumpur, Malaysia
E-mail: wijono@yahoo.com

Abstract: An analytical calculation of the magnetic field of a cylindrical permanent magnet linear generator is presented. The generator utilises a discrete Halbach permanent magnet array as magnetic field source. The array is constructed of permanent magnets that have a non-uniform length. To solve the governing equations, a direct solution method is used. The flux distributions in the air gap, inside the permanent magnet and in the shaft are calculated. Solutions that are derived using this method are compared with that obtained from the finite element analysis simulation method. Another method is also used in the field calculation, and the result is presented for comparison.

1 Introduction

A linear generator is a compact machine that has a minimal number of components. Its simple construction stems from the fact that the linear electrical generator is directly connected to the prime mover without any transmission means. Since it has fewer moving components than its rotary counterpart, losses are expected to be lower and therefore the overall machine efficiency should be higher.

The machine may be driven by any linear prime mover such as a free piston internal combustion engine or a Stirling engine. The power output varies from a few milliwatts generated by a torch light up to several megawatts generated by a tidal wave power generator. A linear generator can be utilised as a stand-alone electrical power supply or an integrated part of a power generation system.

Unlike rotary machines, limited publications on linear generator indicate that there are still a lot of areas related to linear generators that can be explored for further research and development. A typical analysis of the field distribution of the linear machine is presented in [1, 2]. Analyses may also be adapted from the rotary machine methods presented in [3–5] after they are converted to linear systems.

This paper presents a calculation of the flux distribution in a linear permanent magnet generator. Maxwell's equations are used to compute magnetic field quantities in all parts of the machine. The existence of permanent magnet as a free magnetic source is represented by the Poisson's equation. Two general methods are commonly used to solve this equation, that is, it can either be solved directly, which is based on the equation pattern, or by the help of the surface integral form of the permanent magnets to represent the magnetic field source. One of the direct solutions uses an exponential function [6]. The examples of analysis that are adopted in this paper are presented in [1, 2, 7–10]. One of the advantages of using the direct solution is that it does not require the surface integral form to represent the magnetic source which may has a complicated shape, and therefore the Poisson's equation is solved while treating the magnets in whole.

Instead of using the exponential form combined with hyperbolic sine function as presented in [6], this paper employs the Struve function to solve the Poisson's equation. Similar in usage to the Bessel function, the Struve function is used to solve governing equations of the system which has free magnetic sources.

A finite element method simulation is performed to validate results obtained by the proposed method. Taking

advantage of the machine shape, a 2D axisymmetry finite element analysis (FEA) model is set up to simplify the simulation.

2 Machine construction

The linear generator prototype is shown in Fig. 1. The machine is constructed of a stator and a translator, as shown in Fig. 2. Six windings are placed in the slotted stator core. Seven pieces of permanent magnets are mounted on a non-permeable translator shaft to produce the magnetic field. Those permanent magnets are arranged in a discrete Halbach array, that is, radially magnetised permanent magnets (RMPMs) and axially magnetised permanent magnets (AMPMs) are stacked alternately.

A discrete Halbach permanent magnet construction offers some advantages over the conventional Halbach magnet. It is considered due to the fact that local manufacturers do not have the capability to produce the conventional Halbach array in a single piece. On the other hand, the discrete Halbach permanent magnet also offers a lower cost besides it is easy to manufacture.

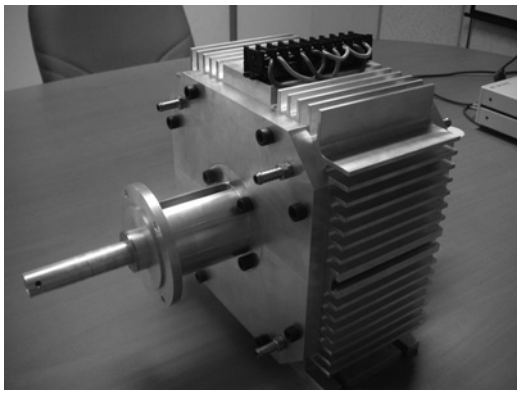

Figure 1 *Linear generator prototype*

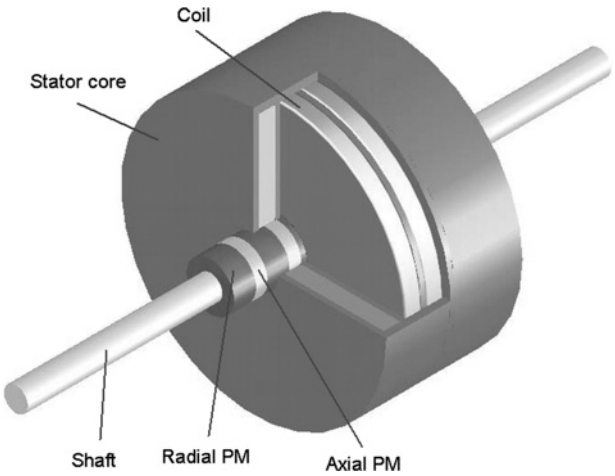

Figure 2 *Linear generator construction*

The machine runs in a reciprocating linear motion. The system produces a linear three-phase output voltage. It is not a real three-phase output like in the rotary machine, since the machine runs forward and then moves backward after it reaches the end of the motion. A long-translator machine is the type selected for better overall performance.

3 Modelling and analysis

The 2D cross-section of the upper half of the machine is shown in Fig. 3. It is divided into three regions where region 1 consists of the air gap and windings, region 2 includes the permanent magnet set and region 3 represents the shaft. The division is based on the permeability of the component material. The region numbers are noted as a subscript in all equations. The machine specification is listed in Table 1. The machine dimension is provided from the actual optimised construction and is intended for the simulation and the analysis only. The optimisation to obtain the machine dimension is not presented.

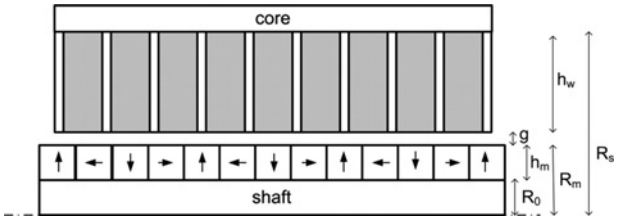

Figure 3 *Cross-section of the upper half of the linear generator*

Table 1 Generator specification

Parameter	Value
speed	3000 stroke per minute
stroke	69 mm
shaft radius, R_0	12.5 mm
magnet height, h_m	12 mm
winding height, h_w	102 mm
AMPM length	12 mm
RMPM length	22.5 mm
air gap	1 mm
slot width	17 mm
teeth width	6 mm
remanent magnetisation, B_{rem}	1.12 T
relative permeability of shaft material, $\mu_{r,shaft}$	1
permeability of core material $\mu_{r,core}$	infinity

doi: 10.1049/iet-epa.2009.0267

The governing equations are built with the following assumptions for simplification. First, the machine is analysed without the stator slot. In the flux linkage calculation, the slots effect is usually incorporated by applying the Carter coefficient. Second, the machine is assumed to be infinitively long and has a periodic construction. Third, the permeability of the stator core is assumed to be infinite whereas the relative permeability of the winding, air gap and permanent magnet as well as the shaft is assumed to be one.

Maxwell's and Poisson's equations for zones 1, 2 and 3 are, respectively, given as

$$\nabla^2 \boldsymbol{A}_i = 0 \quad \text{for} \quad i = 1, 3 \tag{1}$$

$$\nabla^2 \boldsymbol{A}_2 = -\mu_0 \nabla \times \boldsymbol{M} \tag{2}$$

The vector potential $\boldsymbol{A}$ has only one component, A_θ, which is independent of θ in the cylindrical system. Therefore (1) and (2) can be written as

$$\frac{\partial}{\partial z}\left(\frac{1}{r}\frac{\partial}{\partial z}(rA_{i\theta})\right) + \frac{\partial}{\partial r}\left(\frac{1}{r}\frac{\partial}{\partial r}(rA_{i\theta})\right) = 0 \quad \text{for} \quad i = 1, 3 \tag{3}$$

$$\left[\frac{\partial}{\partial z}\left(\frac{1}{r}\frac{\partial}{\partial z}(rA_{2\theta})\right) + \frac{\partial}{\partial r}\left(\frac{1}{r}\frac{\partial}{\partial r}(rA_{2\theta})\right)\right]\boldsymbol{e}_\theta = -\mu_0 \nabla \times \boldsymbol{M} \tag{4}$$

The remanent magnetisation vector can be written in the form of its components $\boldsymbol{M} = M_r\boldsymbol{e}_r + M_z\boldsymbol{e}_z$, where $M_r\boldsymbol{e}_r$ represents the contribution of RMPM and $M_z\boldsymbol{e}_z$ represents the contribution of AMPM. The flux density $\boldsymbol{B}$ obtained from $\boldsymbol{A}$ is given by $Bz = 1/r \cdot \partial/\partial r\ (rA_\theta)$ and $B_r = \partial A_\theta/\partial z$.

In the Fourier series form, the magnetisation vector $\boldsymbol{M}$ is decomposed into harmonics

$$\begin{aligned} M_r &= \sum_{\eta=1,2,\ldots}^{\infty} M_{r\eta} \sin(m_\eta z) \\ M_z &= \sum_{\eta=1,2,\ldots}^{\infty} M_{r\eta} \cos(m_\eta z) \end{aligned} \tag{5}$$

where

$$\begin{aligned} m_\eta &= \frac{(2\eta - 1)\pi}{\tau_{\mathrm{p}}} \\ M_{r\eta} &= \frac{4B_{\mathrm{rem}}}{\mu_0 \tau_{\mathrm{p}} m_\eta} \sin\frac{m_\eta \tau_{\mathrm{p}}}{2} \sin\frac{m_\eta \tau_{mr}}{2} \\ M_{z\eta} &= \frac{4B_{\mathrm{rem}}}{\mu_0 \tau_{\mathrm{p}} m_\eta} \sin\frac{m_\eta \tau_{mz}}{2} \end{aligned} \tag{6}$$

and τ_{p} is the permanent magnet pole pitch, τ_{mr} and τ_{mz} are the length of RMPM and AMPM, respectively.

Therefore (3) and (4) can be written as

$$\frac{\partial}{\partial z}\left(\frac{1}{r}\frac{\partial}{\partial z}(rA_{i\theta})\right) + \frac{\partial}{\partial r}\left(\frac{1}{r}\frac{\partial}{\partial r}(rA_{i\theta})\right) = 0 \quad \text{for} \quad i = 1, 3 \tag{7}$$

$$\frac{\partial}{\partial z}\left(\frac{1}{r}\frac{\partial}{\partial z}(rA_{2\theta})\right) + \frac{\partial}{\partial r}\left(\frac{1}{r}\frac{\partial}{\partial r}(rA_{2\theta})\right) = \sum_{\eta=1,2,\ldots}^{\infty} P_\eta \cos m_\eta z \tag{8}$$

where

$$P_\eta = -\frac{4B_{\mathrm{rem}}}{\tau_{\mathrm{p}}} \sin m_\eta \frac{\tau_{\mathrm{p}}}{2} \sin m_\eta \frac{\tau_{mr}}{2} \tag{9}$$

Boundary conditions are selected to solve the simultaneous field equations, as shown in (10)

$$\begin{aligned} &B_{z1}|r = R_s = 0 \\ &B_{r1}|r = R_m = B_{r2}|r = R_m \\ &B_{r2}|r = R_0 = B_{r3}|r = R_0 \\ &H_{z1}|r = R_m = H_{z2}|r = R_m \\ &H_{z2}|r = R_0 = H_{z3}|r = R_0 \end{aligned} \tag{10}$$

Solving (7) and (8) using boundary conditions in (10) and rearranging them in terms of the vector potential yields

$$\begin{aligned} A_{\theta i} = \sum_{\eta=1}^{\infty} &(C_{\eta i}\,\mathrm{Bessel}\,I_1(m_\eta r) \\ &+ D_{\eta i}\,\mathrm{Bessel}\,K_1(m_\eta r))\cos(m_\eta z) \quad \text{for} \quad i = 1, 3 \end{aligned} \tag{11}$$

$$\begin{aligned} A_{\theta 2} = \sum_{\eta=1}^{\infty} &((C_{\eta 2}\,\mathrm{Bessel}\,I_1(m_\eta r) \\ &+ D_{\eta 2}\,\mathrm{Bessel}\,K_1(m_\eta r))\cos(m_\eta z) + S(r, z)) \end{aligned} \tag{12}$$

where Bessel I_1 is the modified Bessel function of the first kind of order 1 and Bessel K_1 is the modified Bessel function of the second kind of order 1. C and D are constants.

Equation (12) is the general solution of (8), which is a non-homogeneous Bessel's differential equation. Therefore (12) contains Struve functions [11] that exists in the unknown term $S(r, z)$. Solving (8) for $S(r, z)$ yields

$$S(r, z) = \frac{1}{2}\frac{\pi\,\mathrm{Struve}\,L_1(m_\eta r)P_\eta \cos(m_\eta z)}{m_\eta^2} \tag{13}$$

where Struve L_1 is the modified Struve function of order 1.

The flux distributions in all the three regions are derived from (11) and (12), which yield

$$B_{ri} = \sum_{\eta=1,2,\ldots}^{\infty} m_\eta \begin{pmatrix} C_{\eta i}\,\text{Bessel}\,I_1(m_\eta r) + \\ D_{\eta i}\,\text{Bessel}\,K_1(m_\eta r) \end{pmatrix} \sin(m_\eta z)$$
$$\text{for} \quad i = 1, 3 \tag{14}$$

$$B_{zi} = \sum_{\eta=1,2,\ldots}^{\infty} m_\eta \begin{pmatrix} C_{\eta i}\,\text{Bessel}\,I_0(m_\eta r) - \\ D_{\eta i}\,\text{Bessel}\,K_0(m_\eta r) \end{pmatrix} \cos(m_\eta z)$$
$$\text{for} \quad i = 1, 3 \tag{15}$$

$$B_{r2} = \sum_{\eta=1,2,\ldots}^{\infty} \begin{pmatrix} \frac{1}{2}\frac{\pi\ \text{Struve}\ L_1(m_\eta r) P_\eta \sin(m_\eta z)}{m_\eta} \\ + m_n \begin{pmatrix} C_{\eta 1}\,\text{Bessel}\,I_1(m_\eta r) + \\ D_{\eta 1}\,\text{Bessel}\,K_1(m_\eta r) \end{pmatrix} \sin(m_\eta z) \end{pmatrix} \tag{16}$$

$$B_{z2} = \sum_{\eta,1,2,\ldots}^{\infty} \begin{pmatrix} \frac{1}{2}\frac{\pi\ \text{Struve}\ L_0(m_\eta r) P_\eta \cos(m_\eta z)}{m_\eta} \\ + m_\eta \begin{pmatrix} C_{n2}\,\text{Bessel}\,I_0(m_\eta r) - \\ D_{n2}\,\text{Bessel}\,K_0(m_\eta r) \end{pmatrix} \cos(m_\eta z) \end{pmatrix} \tag{17}$$

Equations (14) to (17) represent the field density of the whole machine.

The induced voltage generated in the winding is computed by adding Carter coefficient to represent the existence of the stator slot to the above slotless machine model. This coefficient is given by [1]

$$K_C = \frac{\tau_{sp}}{\tau_{sp} - \gamma g'} \tag{18}$$

where τ_{sp} is the stator slot pitch, and $g' = g + h_m/\mu_r$. The slotting factor γ is given by

$$\gamma = \frac{4}{\pi}\left[\frac{b_0}{2g'}\tan^{-1}\left(\frac{b_0}{2g'}\right) - \ln\sqrt{1 + \left(\frac{b_0}{2g'}\right)^2}\right] \tag{19}$$

where b_0 is the width of the stator slot openings.

The air gap distance should be modified to include the stator slotting effect. The effective air gap is given by

$$g_e = g + (K_C - 1)g' \tag{20}$$

Therefore the stator bore radius should also be recalculated with the effect of slotting incorporated. The equivalent stator bore radius R_{se} is given by

$$R_{se} = R_m + g_e \tag{21}$$

where R_m is the outer radius of the magnets.

The flux linkage of a stator winding is obtained by integrating the vector potential in region 1 over the winding pitch. The total flux linkage of a phase winding is the sum of the flux linkages in all the windings that are connected in series. In this machine, two windings are connected as one phase. Therefore the flux linkage will be

$$\Psi_w = \frac{N_w}{\tau_w(R_s - R_i)}\int_{z-(\tau_w/2)}^{z+(\tau_w/2)}\int_{R_i}^{R_{se}} 2\pi r A_{\theta 1}(r, z)\,dr\,dz \tag{22}$$

Finally, the induced EMF in each phase winding is calculated by

$$e_w = -\frac{d\Psi_w(z)}{dt} = -\frac{d\Psi_w(z)}{dz}v(t) \tag{23}$$

where $v(t)$ is the velocity of the translator as a function of time.

4 Results and discussion

Samples of flux distributions in the three regions are plotted in the subsequent graphs. The respective locations chosen for the regions are as follows:

- Air gap, $r = R_m + g/2$
- Permanent magnets, $r = R_o + h_m/2$
- Shaft, $r = R_o/2$

The equations for the flux density are solved using the direct method with the application of Struve function. The tangential component of the flux density B_z and the radial

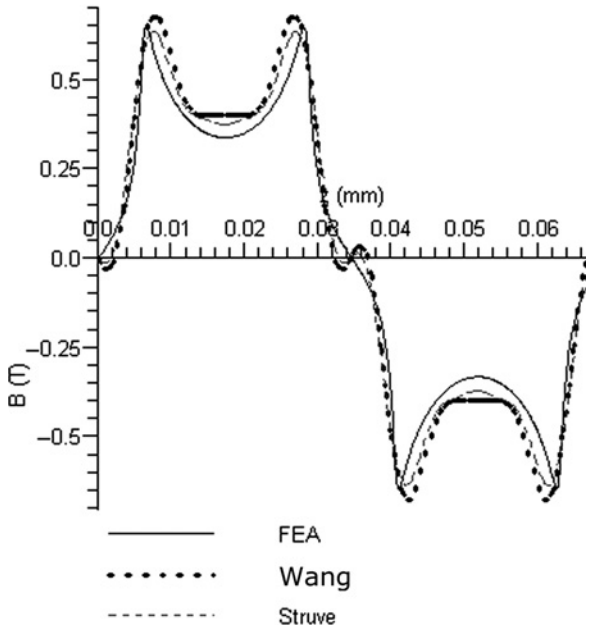

Figure 4 *Radial component of the flux density B_r in the air gap*

doi: 10.1049/iet-epa.2009.0267

component B_r in the air gap, permanent magnet and shaft are plotted in Fig. 4, until Fig. 9. The result is potted against the flux density obtained from the FEA simulation. Another calculation is performed using the equation presented in [1, 2], or other similar papers written by the same author. The result is then plotted in the graph for the comparison of results and labelled by 'Wang'. In these samples, the equation's series is limited to six orders.

The flux linkages in the windings are calculated using the proposed method. The Wang method is also used to calculate quantity, and the results are presented for comparison. The flux linkage and the emf obtained are compared to that computed using the FEA method.

The FEA simulations are performed using Ansoft® Maxwell software [12]. The machine is modelled into the

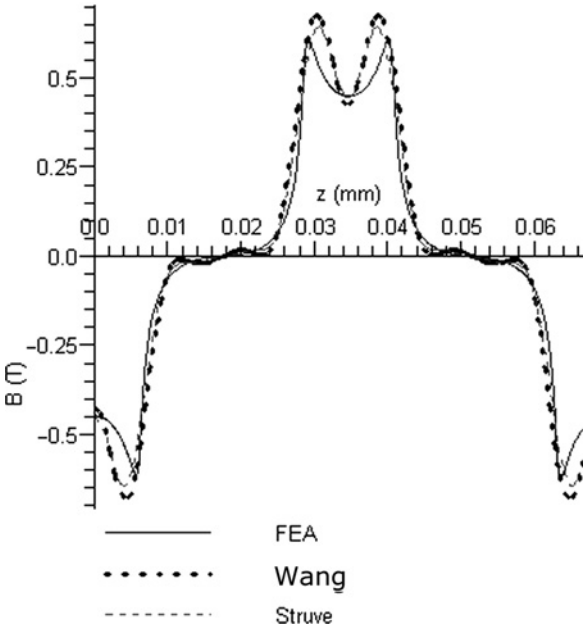

Figure 5 *Axial component of the flux density B_z in the air gap*

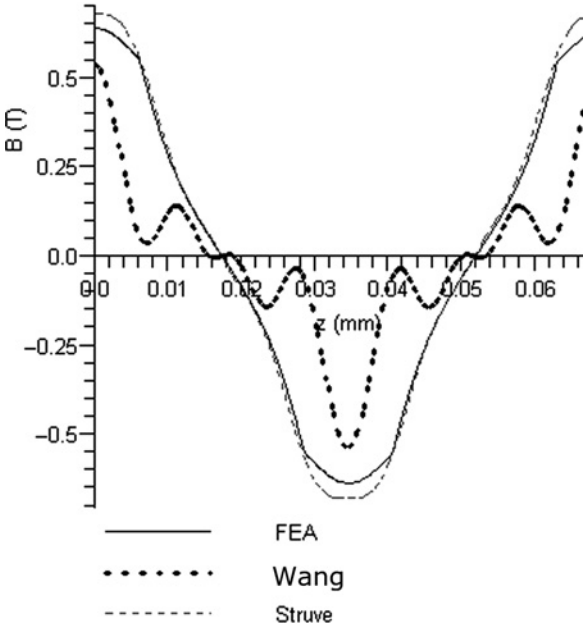

Figure 7 *Axial component of the flux density B_z the permanent magnet*

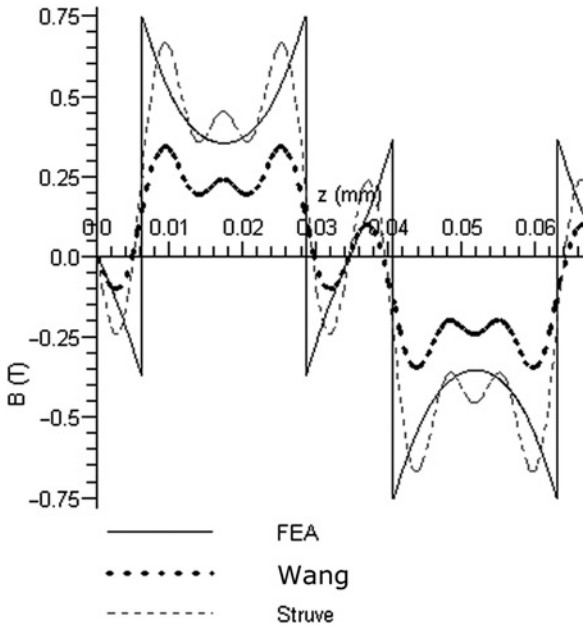

Figure 6 *Radial component of the flux density B_r in the permanent magnet*

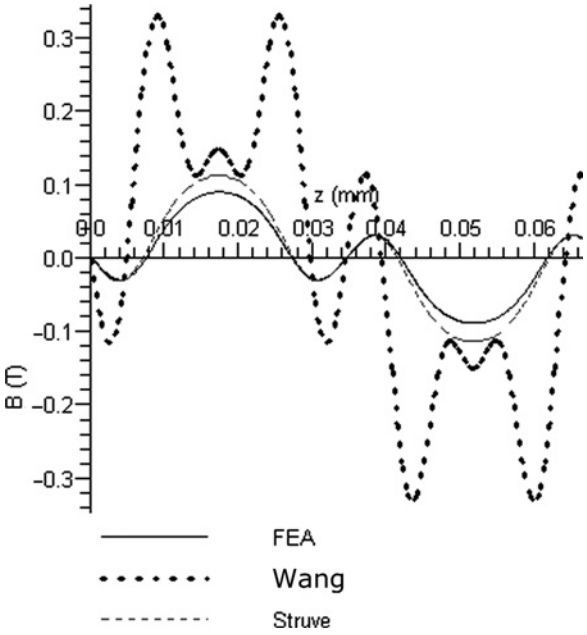

Figure 8 *Radial component of the flux density B_r in the shaft*

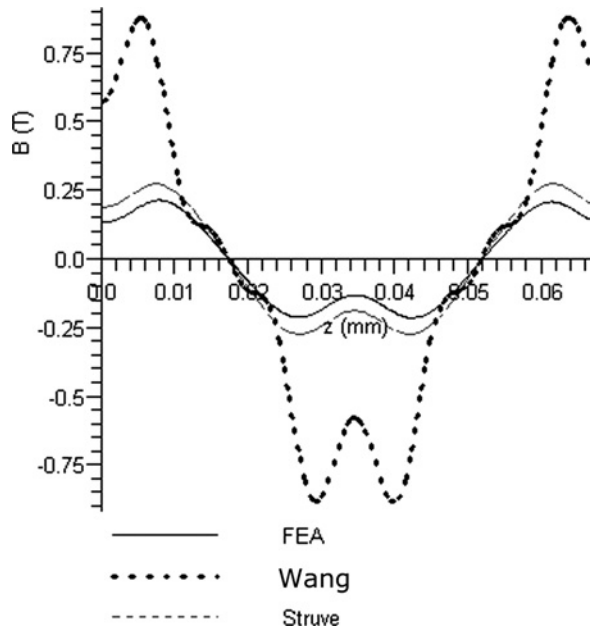

Figure 9 *Axial component of the flux density B_z in the shaft*

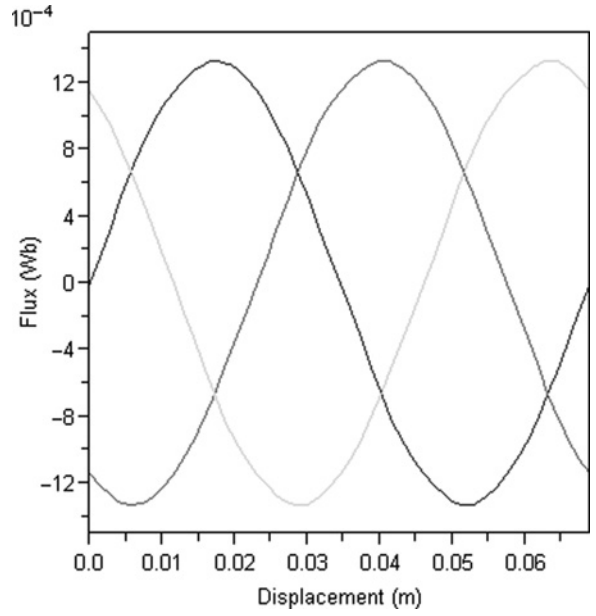

Figure 10 *Three-phase flux linkages calculated with the Struve method*

simulation object. Taking advantage of the symmetrical construction, the machine is modelled with 2D object as shown in Fig. 3. Object properties are provided in Table 1. A circular simulated infinity boundary is drawn to cover the objects. The size is approximately 5 times bigger than the object. A high-density meshing is applied to the components, especially to the air gap. It offers an accurate calculation during the simulation. The parametric simulations are performed to compute the flux distribution in the machine. This simulation method is also used to calculate the induced voltage, since the existing software does not offer the transient simulation feature.

In Figs. 4 and 5, it is noted that the calculated flux densities in the air gap produced by Struve and Wang method are very similar to the one generated by the FEA simulation. Figs. 6 and 7 show the flux densities in the permanent magnets, as produced by the Struve, Wang and FEA methods. It can be seen that the flux densities of the proposed method is much closer to that of the FEA than the one generated by Wang method.

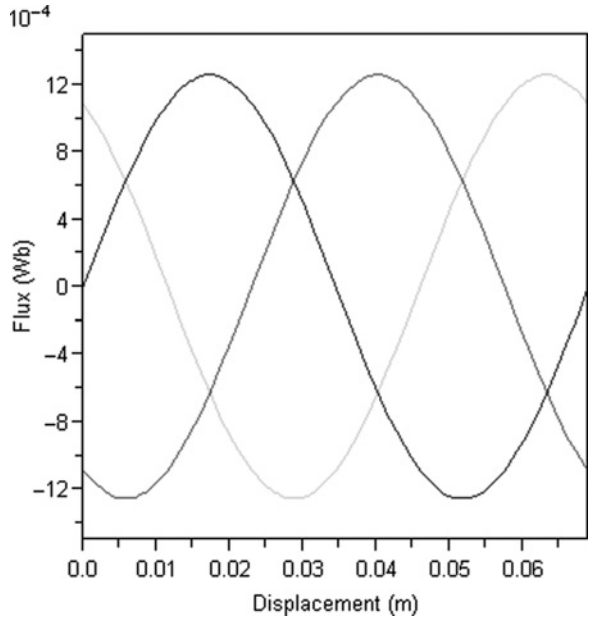

Figure 11 *Three-phase flux linkages calculated with the Wang method*

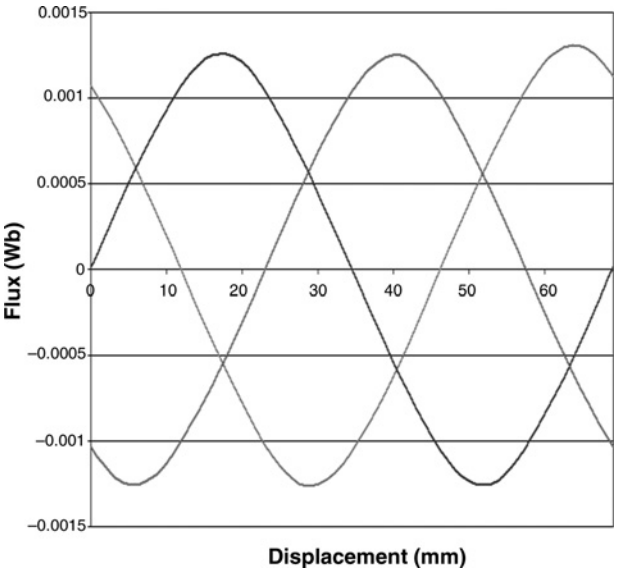

Figure 12 *Three-phase flux linkages calculated with the FEA method*

doi: 10.1049/iet-epa.2009.0267

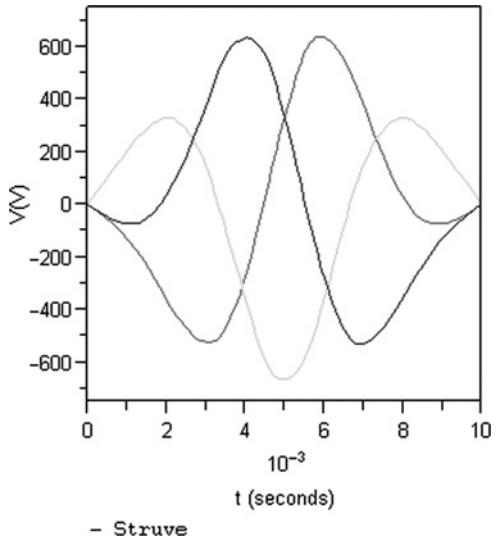

Figure 13 *Three-phase induced voltage calculated with the Struve method*

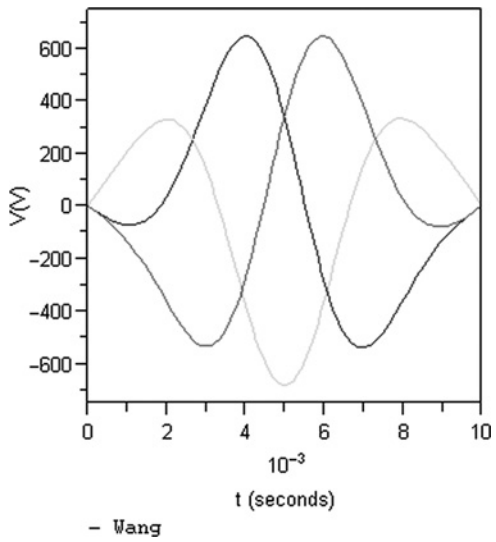

Figure 14 *Three-phase induced voltage calculated with the Wang method*

In the shaft, as shown in Figs. 8 and 9, the flux densities calculated by the proposed method is shown to be superior to the result of Wang method; both are relative to the result produced by the FEA method.

The flux linkages are separately plotted in Figs. 10–12 and the induced voltages are shown in Figs. 13–15. In Fig. 12 the flux linkage is plotted for all windings. The flux linkage profiles calculated using the proposed method match the one generated by FEA. It appears that results from the proposed method and Wang method are very close to each other.

The induced voltage waveforms calculated by the proposed method also bode well with the one calculated using the

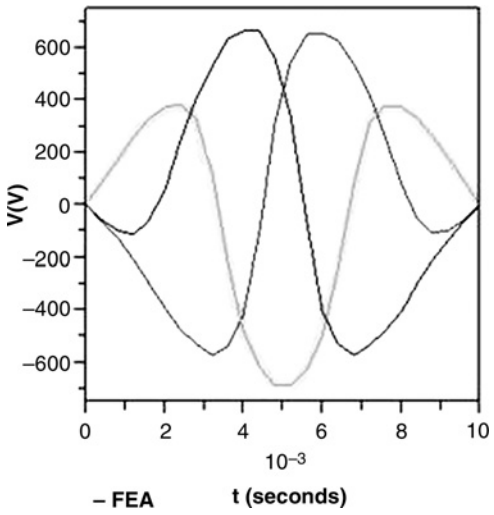

Figure 15 *Three-phase induced voltage calculated with the FEA method*

FEA. This is also true for one calculated by the Wang method.

In conclusion, the close agreement of the results of the direct method and the FEA simulation vindicates the validity of this approach. It has been shown that the method presented in this paper can be used as a tool for field estimation and design optimisation in the machine design.

5 Conclusions

The analytical calculation of the open circuit magnetic field of a cylindrical permanent magnet linear generator equipped with a discrete Halbach permanent magnet array is presented in this paper. A direct solution to the governing equation for the machine is outlined. The Poisson's equation derived has a non-homogenous Bessel's differential equation pattern, which can be solved directly using Struve function. The method offers an exact solution to the field density equation in the machine.

Plots of the results show that the solutions match those produced by the FEA simulation very closely.

6 Acknowledgments

The authors gratefully appreciate and thank the Ministry of Science, Technology and Environment, Malaysia, for the funding of this research project under IRPA Grant No. 33-02-03-3013.

7 References

[1] WANG J., HOWE D.: 'Tubular modular permanent-magnet machines equipped with quasi-Halbach magnetized magnets – part I: magnetic field distribution, EMF, and thrust force', *IEEE Trans. Magn.*, 2005, **41**, (9), pp. 2470–2478

[2] WANG J., JEWELL G.W., HOWE D.: 'A general framework for the analysis and design of tubular linear permanent magnet machines', *IEEE Trans. Magn.*, 1999, **35**, (3), pp. 1986–2000

[3] ZHU Z.Q., HOWE D., XIA Z.P.: 'Prediction of open-circuit air gap field distribution magnet rotor topology in brushless machines having an inset permanent magnet topology', *IEEE Trans. Magn.*, 1994, **30**, (1), pp. 98–107

[4] ZHU Z.Q., HOWE D., BOLTE E., ACKERMANN B.: 'Instantaneous magnetic field distribution in brushless permanent magnet dc motors, Part I: Open-circuit field', *IEEE Trans. Magn.*, 1993, **29**, (1), pp. 124–135

[5] ZHU Z.Q., HOWE D.: 'Instantaneous magnetic field distribution in brushless permanent magnet dc motors, Part III: Effect of armature slotting', *IEEE Trans. Magn.*, 1993, **29**, (1), pp. 143–151

[6] BOLDEA I., NASAR S.A., FU Z.: 'Fields, forces, and performance equations of air-core linear self-synchronous motor with rectangular current control', *IEEE Trans. Magn.*, 1988, **24**, (5), pp. 2194–2203

[7] WANG J., HOWE D.: 'Design optimization of radially magnetized, iron-cored, tubular permanent-magnet machines and drive systems', *IEEE Trans. Magn.*, 2004, **40**, (5), pp. 3262–3277

[8] WANG J., HOWE D., JEWELL G.W.: 'Analysis and design optimization of an improved axially magnetized tubular permanent-magnet machine', *IEEE Trans. Energy Convers.*, 2004, **19**, (2), pp. 289–295

[9] WANG J., HOWE D., JEWELL G.W.: 'Fringing in tubular permanent-magnet machines: part I. Magnetic field distribution, flux linkage, and thrust force', *IEEE Trans. Magn.*, 2003, **39**, (6), pp. 3507–3516

[10] WANG J., HOWE D.: 'A linear permanent magnet generator for a free-piston energy converter'. Proc. IEEE Int. Conf. on Elect. Mach. and Drives, San Antonio, TX, 15 May 2005, pp. 1521–1528

[11] ABRAMOWITZ M., STEGUN I.A.: 'Handbook of mathematical functions' (National Bureau of Standards, Washington, DC, 1972, 10th Printing) pp. 496–502

[12] http://www.ansoft.com, accessed February 2010

doi: 10.1049/iet-epa.2009.0267